A Configurable Energy-Efficient Compressed Sensing Architecture With Its Application on Body Sensor Networks

Aosen Wang, *Student Member, IEEE*, Feng Lin, *Member, IEEE*, Zhanpeng Jin, *Member, IEEE*, and Wenyao Xu, *Member, IEEE*

***Abstract*—The past decades have witnessed a rapid surge in new sensing and monitoring devices for well-being and healthcare. One key representative in this field is body sensor networks (BSNs). However, with advances in sensing technologies and embedded systems, wireless communication has gradually become one of the dominant energy-consuming sectors in BSN applications. Recently, compressed sensing (CS) has attracted increasing attention in solving this problem due to its enabled sub-Nyquest sampling rate. In this paper, we investigate the quantization effect in CS architecture and argue that the quantization configuration is a critical factor of the energy efficiency for the entire CS architecture. To this end, we present a novel configurable quantized compressed sensing (QCS) architecture, in which the sampling rate and quantization are jointly explored for better energy efficiency. Furthermore, to combat the computational complexity of the configuration procedure, we propose a rapid configuration algorithm, called RapQCS. According to the experiments involving several categories of real biosignals, the proposed configurable QCS architecture can gain more than 66% performance-energy tradeoff than the fixed QCS architecture. Moreover, our proposed RapQCS algorithm can achieve over $150\times$ speedup on average, while decreasing the reconstructed signal fidelity by only 2.32%.**

***Index Terms*—Body sensor networks (BSNs), compressed sensing (CS), configurable architecture, quantization effect, RapQCS.**

I. Introduction

WITH THE recent advances in sensing and computer technology, body sensor networks (BSNs) have been widely applied in various domains, such as long-term healthcare telemonitoring [1], sports enhancement [2], and assisted rehabilitation [3]. Energy efficiency is becoming one of the most challenging issues in BSN system [4]. Due to the scaling of data throughput with the development of hardware and computing technology, wireless transmission has become the dominant energy consumer in the entire BSN system [5]. In recent years, the compressed sensing (CS) theory [6] provides a breakthrough paradigm to tackle the energy-efficiency challenge in wireless communication. The CS theory guarantees an accurate recovery by sampling the signals at a lower rate, which is proportional to their intrinsic salient information, rather than their bandwidths. By breaking the limitation of the traditional Shannon–Nyquist sampling theorem, CS brings great potential to dramatically reduce the power consumption on wireless transmission. Furthermore, with the integration of the sampling and compression procedures, the CS framework would also be beneficial to the applications in size, weight, and power-constrained environments.

In 2004, Donoho first officially introduced the concept of CS [6]. In 2006, Candes and Tao proved robust uncertainty principles in CS [7]. With the superior advantage of energy efficiency, the CS framework has been successfully applied to many different fields. Duarte *et al.* [8] designed a single pixel camera based on CS, and Wright *et al.* [9] employed the CS theory for face recognition to reach astonishing results. However, some fundamental technical challenges in the practice of CS in BSN system remain unsolved. One of the concerns is that analog signals in modern computing systems must be digitized before wireless transmission. The quantization effect in CS is still under-explored regarding the energy-performance tradeoff. For example, different sectors in a BSN system emphasize different design criteria. Specifically, distributed body sensors are usually energy bounded, and more sensitive to energy consumption, while data aggregators compile data quality.

In this paper, we propose and investigate a novel configurable quantized compressed sensing (QCS) architecture. In addition to the sampling rate, also referred to as the compression ratio, QCS integrates the quantization operation in practice into the CS-base data flow. Based on extensive experiments, we have proved that the quantization configuration is a critical and sensitive factor in the QCS architecture for its energy efficiency. We develop the energy model for the configurable QCS architecture to quantitatively evaluate its performance–energy (P–E) tradeoff in both architecture- and circuit-level design space. Moreover, we develop a rapid configuration algorithm, called RapQCS, to further reduce the elapsed time while compromising virtually no performance deviation of the QCS architecture.

Manuscript received September 04, 2014; revised December 18, 2014, March 10, 2015, May 29, 2015, July 01, 2015, and September 01, 2015; accepted September 13 2015. Date of publication September 28, 2015; date of current version February 02, 2016. This work was supported by the National Science Foundation under Grant CNS-1423061/1422417, Grant ECCS-1462498/146247, and Grant CNS-1547167. Paper no. TII-14-0985.

A. Wang, F. Lin, and W. Xu are with the Department of Computer Science and Engineering, State University of New York at Buffalo, Buffalo, NY 14260 USA (e-mail: aosenwan@buffalo.edu; flin28@buffalo.edu; wenyaoxu@buffalo.edu).

Z. Jin is with the Department of Electrical and Computer Engineering, Binghamton University, State University of New York, Binghamton, NY 13902 USA (e-mail: zjin@binghamton.edu).

Color versions of one or more of the figures in this paper are available online at http://ieeexplore.ieee.org.

Digital Object Identifier 10.1109/TII.2015.2482946

In this work, our main contributions are threefold.

1) We propose a configurable QCS architecture, which considers both the sampling rate and quantization configuration. We analyze the significance of the quantized bit resolution in the CS framework, and prove that the optimized quantization configuration with the sampling rate can provide a better P–E tradeoff.
2) We develop a RapQCS algorithm to quickly locate the optimal configuration of the sampling rate and the bit resolution, with a bound energy budget in practice, which can drastically reduce the elapsed time while keeping an excellent efficiency and capacity of the QCS.
3) We evaluate the QCS architecture with experiments using biosignal data sets. The configurable QCS architecture can improve the P–E tradeoff by more than 66%. Meanwhile, our fast RapQCS algorithm can offer $150\times$ speedups while introducing a 2.32% average distortion rate.

This paper is organized as follows. Section II introduces prior work of CS and quantization. The basics of conventional CS theory are described in Section III. Our proposed efficient QCS architecture is elaborated in Section IV, and Section V presents our fast RapQCS algorithm. Related experiments and evaluations are discussed in Section VI, and Section VII presents our conclusion and future work.

II. Related Work

Most research on CS is focused on the reconstruction algorithms to pursue lower sampling rate and better signal quality. Reconstruction algorithms comprise three categories [10]: greedy algorithm, convex optimization, and iterative thresholding. Greedy algorithm aims to select the most significant components in sparsity-inducing bases, such as orthogonal matching pursuit (OMP) and compressive sampling matching pursuit (CoSaMP). The convex optimization method is based on optimizing the ℓ_1 norm problem and its variants. Representatives include basis pursuit (BP), NESTA, and gradient projection. Iterative thresholding can solve the ℓ_1 penalized least square problem with fast speed, such as iterative splitting and shareholding (IST) and iterated hard shrinkage (IHT). Also, Liu *et al.* implemented an energy-efficient reconstruction algorithm on a field-programmable gate array (FPGA) [11]. Although these reconstruction algorithms can either reduce the measurements dimension or improve the reconstruction accuracy, they ignore that quantization is an inevitable process when applying CS into practical applications.

There are some existing work that take quantization effects into account. Dai *et al.* [12] studied the quantization effects on reconstruction error of CS. Laska *et al.* [13] mitigated the quantization effects by adapting the CS reconstruction algorithm. Also, an optimal quantizer was designed [14] for the least absolute shrinkage and selection operator (LASSO) reconstruction under high-resolution quantization assumption. All aforementioned research primarily focus on reducing the quantization noise or mean-square quantization error (mse) by designing a better quantizer. However, understanding the quantization effect on compressed signals is not typically a research priority. Fauvel *et al.* presented a comprehensive analysis of electroencephalography (EEG) telemonitoring architecture in [15], but took the bit resolution of quantization operation as a constant value. In fact, the quantization effort on reconstruction error is indeed related to the overall system performance. Moreover, researchers did not investigate the impacts of the quantization effect on energy consumption in BSN applications.

III. Background of CS

CS is an emerging low-rate sampling scheme for the signals that are known to be sparse or compressible in certain cases. CS has been successfully applied in image processing, pattern recognition, and wireless communications.

We assume $\boldsymbol{x}$ is an N-dimensional vector and sampled using M-measurement vector $\boldsymbol{y}$

$$\boldsymbol{y} = \Phi \boldsymbol{x} \tag{1}$$

where $\Phi \in R^{M\times N}$ is the sensing array, which models the linear encoding, and M is defined as the sampling rate in N-dimensional CS. The elements in Φ are either Gaussian random variables or Bernoulli random variables. Because of $M << N$, the formulation in (1) is undetermined, and signal $\boldsymbol{x}$ cannot be uniquely retrieved from sensing array Φ and measurements $\boldsymbol{y}$. However, under a certain sparsity-inducing basis $\Psi \in R^{N\times N}$, the signal $\boldsymbol{x}$ can be represented by a set of sparse coefficients $\boldsymbol{u} \in R^N$

$$\boldsymbol{x} = \Psi \boldsymbol{u} \tag{2}$$

i.e., the coefficient $\boldsymbol{u}$, under the transformation Ψ, only has few nonzero elements. Therefore, based on (1) and (2), the sparse vector $\boldsymbol{u}$ can be represented as follows:

$$\boldsymbol{y} = \Phi\Psi\boldsymbol{u} = \Theta_{M\times N}\boldsymbol{u} \tag{3}$$

where $\Theta_{M\times N} = \Phi\Psi$ is an $M \times N$ array, called measuring matrix. Due to the prior knowledge that the unknown vector $\boldsymbol{u}$ is sparse, it is possible to estimate the value $\boldsymbol{u}$ using the ℓ_0 minimization formulation as follows:

$$\boldsymbol{u} = \min \|\boldsymbol{u}\|_0, \quad \text{s.t. } \|\boldsymbol{y} - \Theta\boldsymbol{u}\| < \epsilon \tag{4}$$

where ϵ is the reconstruction error tolerance. The formulation in (4) is a determined system with unique solutions. However, ℓ_0 is an NP-hard problem [16], and one of the methods to solve (4) is to approximate ℓ_0 minimization formulation to ℓ_1 minimization formulation

$$\boldsymbol{u} = \min \|\boldsymbol{u}\|_1, \quad \text{s.t. } \|\boldsymbol{y} - \Theta\boldsymbol{u}\| < \epsilon. \tag{5}$$

Under the condition of restricted isometry property (RIP) [17], ℓ_1 has been theoretically proven to be equivalent to minimize ℓ_0. Moreover, ℓ_1 minimization is convex and can be solved within polynomial time. In this work, we will use the ℓ_1-based approach CS. After estimating the sparse coefficient $\boldsymbol{u}$ with the formulation in (5), the original input signal $\boldsymbol{x}$ can be recovered directly

$$\dot{x} = \Psi\boldsymbol{u}. \tag{6}$$

TABLE I
NOTATIONS AND SYMBOLS IN THIS PAPER

Notation or symbol	Description
$\boldsymbol{x}$	High-dimension raw analog signal
$\boldsymbol{y}$	Low-dimension compressed measurements from randomized encoding
Φ	Sensing array modeling the randomized encoding
$\boldsymbol{u}$	Sparse representation of signal x under sparsity-inducing basis
Ψ	sparsity-inducing basis for the original analog signal x
Θ	Measuring Matrix combining the sensing matrix Φ and sparsity-inducing basis Ψ
ϵ	Small positive threshold indicating error tolerance
$\dot{x}$	Reconstruction result under traditional CS framework
$\widehat{y}$	Quantized random measurements
Q_b	Quantization function with b as its bit resolution
$\widehat{u}$	Sparse representation estimation based on quantized measurements $\widehat{y}$
$\widehat{x}$	Original signal reconstruction result based on quantized measurements $\widehat{y}$
M	Sampling rate in randomized encoding module
b	Bit resolution in quantization module
C	Constant decided by specific wireless communication technique
E	Energy model of our proposed QCS architecture
$P(M,b)$	Performance metric of the architecture under specific parameter configuration, M and b
E_0	Energy bound, a predefined energy level value according to specific requirements
$(M,b)_{\text{opt}\|\text{cst}}$	The optimal parameter configuration under specific constraints cst
$(M,b)_{\min}$	Parameter configuration corresponding to the lowest energy level
D_E	The set of all possible parameter configurations
G_E	The set of parameter configuration of all performance-energy trade-off points
p_i	Specific parameter affecting energy or performance of QCS, such as M or b
A	Parameter space of all the parameters p_i. It only includes the parameter categories.
s_d	The dth value of a specific parameter p_i
L	Value number of a specific parameter p_i
l	The neighbor distance in RapQCS algorithm
f_c	The cost function of the optimization in RapQCS algorithm
$\boldsymbol{a}$	A specific parameter configuration vector from set A
$N_d(\boldsymbol{a})$	The neighborhood with maximal d distance for parameter vector $\boldsymbol{a}$
$\sigma(\boldsymbol{a})$	The sensitivity of parameter vector $\boldsymbol{a}$
H	The application set supported by our QCS architecture, such as the sensing of ECG, EEG and etc..
h	A specific application from application set H
$\boldsymbol{a}_{opt}(h, \text{EB})$	The optimal parameter configuration of application h under energy bound EB
$\|.\|_z$	The z-norm function, z can be 1, 2 and even ∞
$\rightarrow$	The new neighborhood indicator defined in this paper
$\perp$	Invalid value, not existing

We can see that both reconstruction error and wireless communication energy in the traditional CS formulation are determined by the sampling rate M. Researchers only consider adapting M with regard to different design constraints.

IV. CONFIGURABLE QUANTIZED CS ARCHITECTURE

We first list all the notations and symbols in Table I, for the following discussions of our proposed architecture, and then introduce our proposed configurable QCS framework and related optimization strategy in details.

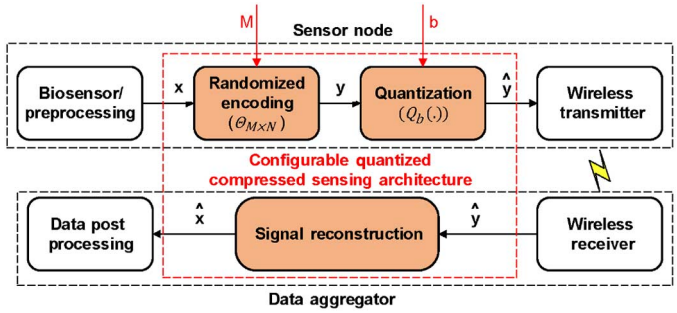

Fig. 1. Configurable quantized CS architecture in BSN. The QCS includes three modules. Randomized encoding, quantization, and signal reconstruction.

A. Architecture Overview

The traditional CS theory does not apply quantization to the formula [see (3)]. In practical applications, original signals are analog in nature and need to be quantized before transmitting over the wireless channel. Therefore, the compressed signal $\boldsymbol{y}$ should be processed by a quantization model formulated as follows:

$$\widehat{y} = Q_b(\boldsymbol{y}) \tag{7}$$

where $Q_b(\cdot)$ is the quantization function, and $\widehat{y}$ is the quantized representation of $\boldsymbol{y}$ with b bits [18]. When considering the quantization process into the CS architecture, the CS formulation is reformulated

$$\widehat{u} = \min \|\boldsymbol{u}\|_1, \quad \text{s.t. } \|\widehat{y} - \Theta\boldsymbol{u}\| < \epsilon. \tag{8}$$

By solving the formulation in (8), we can obtain the sparse representation $\widehat{u}$ from the quantized measurement $\widehat{y}$. Therefore, the reconstructed signal $\widehat{x}$ is retrieved by

$$\widehat{x} = \Psi\widehat{u}. \tag{9}$$

The sensing framework based on the formulation in (8) is defined as QCS architecture, which is illustrated in Fig. 1.

The entire block diagram is a BSN framework, incorporating two key parts. on-body sensor node and data aggregator. The on-body sensor node collects the vital biosignals and implements simple yet necessary signal processing. Then, it sends the data to the data aggregator. The data aggregator can be a local server or remote cloud center to retrieve the collected sensing information for postprocessing. In this framework, the sensor node is sensitive to energy consumption due to the limited-life battery supplement, while the data aggregator focuses on the signal reconstruction quality for later analysis. The transceiver of wireless communication is an off-the-shelf module with low power consumption. It consists of a wireless transmitter in the sensor node and a wireless receiver in the data aggregator. Toward the application in BSNs, the transmitter in the sensor node should comply with certain medical specifications [19] and communication standards, such as IEEE 802.15.6 [20].

We can see that the QCS architecture consists of three parts: 1) randomized encoding; 2) quantization; and 3) signal reconstruction modules. Original analog signals, which usually denote the raw analog data $\boldsymbol{x} \in R^N$, coming from

sensors, are encoded into an M-dimensional vector $\boldsymbol{y} \in R^M$, by linear encoding $\Theta_{M\times N}$. Through the quantization scheme $Q_b(\cdot)$, every measurement becomes a certain b-bit digital representation $\widehat{y}$. A wireless transmitter streams these digitized measurement data to the receiver. When the wireless receiver extracts the data from the bit stream, it performs reconstruction algorithms to recover the N-dimensional original input signal $\boldsymbol{x}$ from the quantized M-dimension compressed measurements $\widehat{y}$. The reconstructed signal $\widehat{x}$ is sent to the data postprocessing model for specific applications, such as signal classification, signal demodulation, or signal separation. In this architecture, linear random encoding and quantization modules form a distributed node for the sensor's flexibility. Reconstruction and postprocessing functions are conducted in the data aggregator. Note that as shown in Fig. 1, in this QCS architecture, both sampling rate M in the random encoding module and bit resolution b in the quantization module are configurable. These parameters can be setup according to different applications.

B. Energy and Performance Models in QCS Architecture

In this part, we discuss the energy and performance models in the QCS architecture. The distributed node is energy bound with limited energy budget, and the data aggregator is performance-driven, focusing on the signal quality. In distributed nodes, the power consumption is dominated by wireless communication, and communication energy is proportional to the volume of the data stream. Therefore, its *energy model* can be formulated as follows:

$$E = C \times M \times b \tag{10}$$

where M is the sampling rate, b is the bit resolution in quantization in the QCS architecture, and C is the energy per bit, i.e., the energy consumption of transmitting 1 bit data.[1] We can change the power consumption of distributed nodes through the M and b setup. The larger the M and b, the more the energy consumption in the distributed nodes.

The aim of the data aggregator is to reconstruct the original signal from the streaming compressed data for postprocessing. For the simplicity of presentation, we use the reconstruction error as the performance metric in the data aggregator. Therefore, the *performance model* in the data aggregator can be defined as follows:

$$P(M,b) = \frac{\|\boldsymbol{x} - \hat{x}\|_2}{\|\boldsymbol{x}\|_2} \times 100\% \tag{11}$$

where $P(M,b)$ denotes the performance metric, i.e., the reconstruction error under the configuration of sampling rate M and resolution bit b. $\widehat{x}$ denotes the recovered signal and $\boldsymbol{x}$ is the original input signal. Because $\widehat{x}$ is directly derived from the measure $\widehat{y}$, the performance is affected by the sampling rate M and the bit resolution b. Specifically, M has an impact on the performance of reconstruction algorithms, and b determines the quantization noise in the measures. From the models in (10) and (11), we can see the QCS architecture can reach different energy-performance tradeoffs through the configuration of M and b.

[1]The energy per bit is determined by the wireless communication protocol and is usually a constant.

C. System Design Formulation

In this part, we present the design formulation toward CS-based distributed systems. The distributed sensor nodes are equipped with a capacity-limited battery, and the battery lifetime is usually the design constraint.

Given an energy bound E_0 for the distributed node, the design criterion in the QCS architecture is to find the optimal configuration of M and b such that the energy E is less than E_0, and the reconstruction error is as small as possible. This design formulation can be formulated as follows:

$$(M,b)_{\text{opt}} = \arg\min_{M,b}(P(M,b)), \quad \text{s.t. } C \times M \times b \le E_0 \tag{12}$$

where $(M,b)_{\text{opt}}$ denotes the optimal energy configuration under energy bound E_0. We can see that the total design space in the formulation in (12) is $b \times M$, where b is the bit resolution in the quantization and M is the sampling rate. Note that the objective function is not in an analytic form, and the constraint function is nonconvex. Therefore, it is challenging to efficiently obtain $(M,b)_{\text{opt}}$.

D. Brute Force Algorithm

The most straightforward method to find $(M,b)_{\text{opt}}$ is the brute force method. It is also called exhaustive searching, a general technique enumerating all potential solutions to check if they satisfy the problem's statement. In our challenge, when energy bound E_0 changes from 0 to $b \times M$, we can get a P–E tradeoff point $(M,b)_{\text{opt}}$ on every bound energy. If we connect all of these P–E tradeoff points, they will form an optimal P–E tradeoff curve, called Pareto's curve [21]. Once the Pareto's curve is depicted in the P–E space, we can easily identify the optimal energy configuration $(M,b)_{\text{opt}}$ under any given bound E_0. So we first employ the brute force method to search the entire P–E space for the Pareto's curve and then set the optimal energy configuration under E_0 by looking up the Pareto's curve. In fact, after we give the definitions of energy and performance, this problem can be solved by searching for a series of P–E tradeoff points, which hold the best tradeoff in lower energy intervals. It can be formulated as follows:

$$(M,b)_{\text{opt}}^{i+1} = \arg\min_{M,b} \|E_{\text{opt}}^{i+1} - E_{\text{opt}}^{i}\|, \quad \text{s.t.} \begin{cases} E_{\text{opt}}^{i+1} > E_{\text{opt}}^{i}, \\ P(E_{\text{opt}}^{i+1}) < P(E_{\text{opt}}^{i}) \end{cases} \tag{13}$$

where i is the number of energy bound, $(M,b)_{\text{opt}}^{i}$ is the ith optimal energy configuration, E_{opt}^{i} is the energy level of $(M,b)_{\text{opt}}^{i}$, and $P(E_{\text{opt}}^{i})$ is the performance metric of $(M,b)_{\text{opt}}^{i}$. We execute our searching by the ascending order of energy level. We start from the minimal energy level, and then increase the energy

level gradually. It is common for more than one (M, b) configuration to be on the same energy level, which results from our energy definition. Under this situation, we exhaustively check every possible (M, b) configuration for the optimal tradeoff. That is, we take every energy configuration (M, b) as our candidates, but our searching order is by ascending order of energy values. The entire algorithm is defined as Algorithm 1.

Algorithm 1. Brute Force Algorithm

Input: E_0: given energy bound
D_E: the set of all the parameter configuration
$(M, b)_{min}$: parameter configuration corresponding to the least energy level
$check13(\cdot)$: function to check if configuration satisfies Eq. (13)

Output: G_E: set of configurations of P-E trade-off points.
$(M, b)_{opt|E_0}$: the optimal configuration with energy bound E_0

$G_E = G_E \bigcup (M, b)_{min}$
$(M, b)_{opt} = (M, b)_{min}$
for each (M, b) in D_E **do**:
  If $check13((M, b), (M, b)_{opt})$ **then**
    $G_E = G_E \bigcup (M, b)$
    $(M, b)_{opt} = (M, b)$
  end if
end for

for $(M, b) \in G_E$ **do**
  if $M \times b \leq E_0$ **then**
    $(M, b)_{opt|E_0} = (M, b)$
  else
    $break$
  end if
end for

We can see from the brute force algorithm that we execute reconstruction for each specific parameter configuration. We adopt the second-order cone programming (SOCP) [22] to solve the ℓ_1 optimization problem in signal reconstruction. The SOCP can be solved under the time complexity of $O(N^3)$, where N is the dimension of the signal. Then the time complexity of brute forcing the entire P–E space should be $O(|M| \times |b| \times N^3)$. An example of the brute force algorithm on one EEG recording segment is shown in Fig. 2. Every red point represents a P–E point, located by its energy configuration (M, b) and corresponding performance $P(M, b)$. The green line is the Pareto's P–E curve, connecting all the P–E tradeoff points, which are centered in the blue triangular markers. However, run time of the brute force algorithm increases sharply as the candidate number grows, which can be demonstrated by the above time complexity analysis.

V. Rapid QCS Configuration With a Bound Energy Budget

In practical applications, it is very common that an upper-energy bound is set to constraint the system's energy consumption. For our proposed configurable QCS architecture, the energy bound is usually set on the distributed node for its sensitivity to power consumption. It is a big challenge to quickly locate the optimal energy configuration under a given energy bound. In the following part, we discuss this challenge and demonstrate how we overcome it.

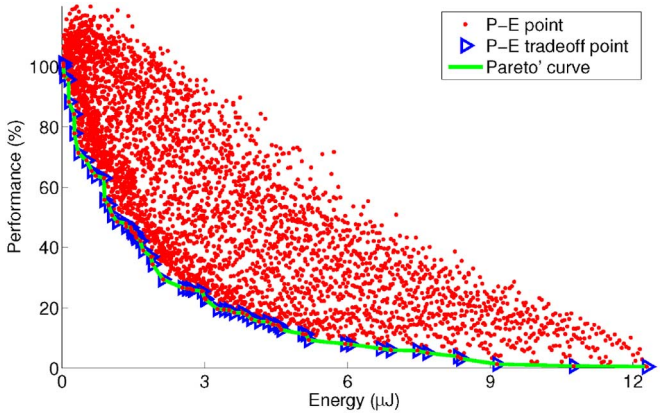

Fig. 2. Brute force algorithm on one EEG recording segment. Red point indicates a P–E point. Blue triangular marks a P–E tradeoff point. Green line is the Pareto's curve.

A. Energy-Efficiency Control Formulation

When there is an energy budget E_0 for the distributed node, it is critical to find an optimal energy configuration corresponding to the best performance under a given constraint. This problem has been formulated in (12), which is an NP-hard problem without any polynomial optimal solutions. The performance in (12) refers to ℓ_0 form, which has been proved to be NP-hard [16], for its optimal solution. An intuitive solution is to apply a brute force algorithm based on ℓ_1 relaxation, whose energy is limited in the bound E_0, to search the subspace entirely. But this method is time consuming and impractical for large-scale problems. Based on our empirical estimation, the energy level where the optimal configuration is located should be just near the energy bound. Thus, it seems not to be a wise way to search the whole bound energy space. In the next section, we will introduce a better heuristic local search algorithm based on the sensitivity analysis to quickly locate the optimal configuration.

B. RapQCS Algorithm

In our QCS architecture, better performance under a given energy budget is the ultimate goal. So, we directly take the performance definition as the cost function f_c of our optimization in RapQCS, assuming a is a specific parameter configuration

$$f_c(\boldsymbol{a}) = P(M, b) = \frac{\|\boldsymbol{x} - \widehat{x}\|_2}{\|\boldsymbol{x}\|_2} \times 100\%. \tag{14}$$

The cost function f_c is a multivariable function. To efficiently tackle this problem, the main idea of our sensitivity analysis is to search for a series of parameter configurations $\boldsymbol{a}_n$ satisfying

$$f_c(\boldsymbol{a}_0) < f_c(\boldsymbol{a}_1) < \cdots < f_c(\boldsymbol{a}_n). \tag{15}$$

By (15), it can guarantee that the cost function f_c converges to the optimal (or suboptimal) solution [23]. For the convergence speed, we first define the sensitivity σ at configuration $\boldsymbol{a}_k$

$$\sigma(\boldsymbol{a}_k) = \{f_c(\boldsymbol{a}_k) - f_c(\boldsymbol{a}_{k+1})\}. \tag{16}$$

Our sensitivity is a differentiable value set for all possible adjacent parameter configurations $\boldsymbol{a}_{k+1}$. Our goal is to find the adjacent configuration $\boldsymbol{a}_{k+1}$ corresponding to the steepest sensitivity value, the maximal in σ, for each parameter configuration $\boldsymbol{a}_k$

$$\boldsymbol{a}_{k+1} = \max_{\boldsymbol{a}_{k+1}}(g) \quad \text{s.t. } g \in \sigma(\boldsymbol{a}_k). \tag{17}$$

Therefore, the current challenge is how to find such parameter configuration sequences. Observing that the parameter configuration $\boldsymbol{a}$ relates to two discrete variables, sampling rate M and bit resolution b, we adopt the neighborhood to construct the relationship between the adjacent parameter configuration pairs. That is, we define $\boldsymbol{a}_{k+1}$ as the neighbourhood of $\boldsymbol{a}_k$. Next, we introduce our neighborhood definition for the QCS design space. For simplifying the presentation of parameters' representation, we define a parameter space A in our QCS architecture as

$$A = \{p_1, \ldots, p_i, \ldots, p_n\} \tag{18}$$

where p_i is the ith parameter category affecting energy or performance in the architecture. For example, due to our energy's definition, M and b are two parameter members in this model. Since parameters are all discrete values, we first define a new neighborhood operator "$\rightarrow$" in the same parameter category p_i

$$s_k \rightarrow d = \begin{cases} s_{k+d}, & 1 \le k+d \le L \\ \perp, & \text{otherwise} \end{cases} \tag{19}$$

where s_k is the kth configuration value of specific parameter p_i. L is the dimension of p_i. We name d as the neighbor distance. Then we continue to introduce symbol N_d as the neighborhood set with d as the upper bound of neighbor distance

$$N_d(s_k) = \{s_k \rightarrow l : \ l \le d\}. \tag{20}$$

For example, N_2 indicates that the neighbor distance from the current position is not more than 2 units. By (19), this case is setting d not more than 2. Here, we can rewrite our sensitivity definition by neighborhood representation

$$\sigma(\boldsymbol{a}_k) = \{f_c(\boldsymbol{a}_{k+1}) - f_c(\boldsymbol{a}) : \ \boldsymbol{a}_{k+1} \in N_d\}. \tag{21}$$

We can find from (21) that the total number of sensitivity values on a specific parameter vector depends on the parameter vector dimension $|\boldsymbol{a}|$ and the neighbor distance d. In our BSN application, the parameter set A has two parameters, M and b. Thus, the value of $|\boldsymbol{a}|$ is 2. Assuming we take neighbor distance $d = 1$, we may have $(2d+1) \times (2|\boldsymbol{a}|+1) - 1$, i.e., we have 8 in total, sensitivity values for a specific configuration $\boldsymbol{a}$. So if the local search chooses the most sensitive direction to proceed, which is with the fastest decreasing of the cost function, optimal (or suboptimal) configuration can be achieved eventually.

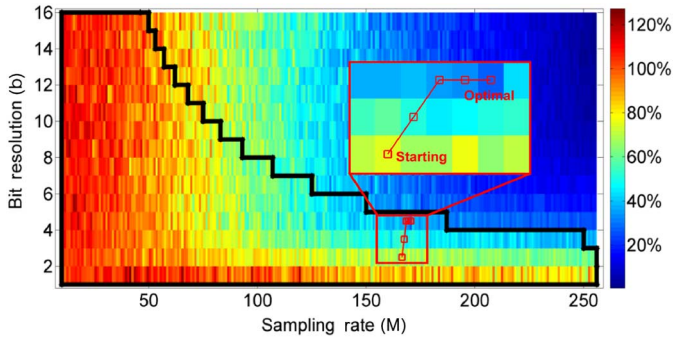

Fig. 3. Example to illustrate the RapQCS algorithm. The colorful blocks indicate the different reconstruction error levels.

For a better convergence speed and a more stable solution, we would like to add a tuning phase to reasonably estimate an initial configuration $\boldsymbol{a}_0$ before the local search based on sensitivity

$$\boldsymbol{a}_0(\text{EB}) = E_{h \in H}(\boldsymbol{a}_{\text{opt}}(h, \text{EB})) \tag{22}$$

where H is the application set. $a_{\text{opt}}(h, \text{EB})$ is the optimal configuration of application h under energy bound EB. In the tuning phase, the brute force algorithm will be employed to search the P–E space for optimal configuration $a_{\text{opt}}(h, \text{EB})$. The entire RapQCS algorithm is defined as Algorithm 2.

Algorithm 2. RapQCS Algorithm

Input: EB:given energy budget
$a_0(EB)$: starting configuration
f_c: cost function
$\sigma(a)$: sensitivity at configuration a
Output: $a_{opt}(EB)$: optimal configuration with EB
1: $a_{opt}(EB) = a_0(EB)$
2: Search for (M, b):

$$(M, b) = arg\min_{M,b}(\sigma(a_{opt})), \quad s.t. \quad \begin{cases} \sigma(a_{opt}) < 0 \\ M \times b < EB \end{cases}$$

3: **if** find such (M, b) **then**
4: $a_{opt}(EB) = (M, b)$
5: *Go to Step* (2)
6: **else**
7: *EXIT*
8: **end if**

Fig. 3 shows an example of the optimal parameter estimation of our RapQCS algorithm. The horizontal axis indicates the sampling rate M, the vertical axis is the bit resolution b, and the small colorful blocks display the different reconstruction error. We can find that reconstruction error has a decreasing trend, blending with fluctuations, as the M and b increase. Specifically, we use black line to delimit the solution space of the brute forcing algorithm under energy budget 2.25 μJ. The brute forcing method needs to probe each parameter setup to search for the optimal solution. We also show the searching path and result of our RapQCS in the small red rectangular area. Note that we zoom in the searching path of

our RapQCS to make the result clearer in the large red rectangular area. We can observe from the zooming-in area that our trained staring point is just near the optimal solution. After several sensitivity propagations, our RapQCS algorithm terminates at the optimal solution. In practice, due to the quality of the starting point estimation, the RapQCS proceeds to the local minimum. For typical biosignals, this local minimum has a 31.39%–47.88% probability to hit the global minimum. We would like to demonstrate why our RapQCS is so rapid. The brute force algorithm and RapQCS have the same run time for the probing with the specific parameter setup (M, b). This is an ℓ_1 minimization-based signal reconstruction attempt using the second-order cone programming strategy [22], whose time complexity is $O(N^3)$, where N is the length of the original input signal. However, the brute force algorithm needs to calculate all the possible parameter combinations under a specific energy constraint, whose size is $O(|M| \times |b|)$, just as delimited by the black line in Fig. 3. For our RapQCS, it starts with a reasonable estimation from (22), and forward to the optimal solution by the steepest performance-changing direction. Our method jointly optimizes the two parameters, sampling rate M and bit resolution b, to come to the convergence, resulting in its linear searching steps $O(s)$, where s is less than 10 empirically. Therefore, our RapQCS algorithm can drastically reduce the run time while keeping the signal quality.

VI. Experiments

A. Experimental Setups and Data Sets

In this section, we describe the performance evaluation on our work from two aspects.

1) We evaluate the advantage of the configurable QCS architecture and compare the P–E tradeoff gain against the traditional CS architecture.
2) We test the effectiveness and efficiency of our RapQCS algorithm, i.e., the reconstruction error, energy-bound accuracy, and runtime speedup, by comparing with the brute force method.

Our configurable QCS architecture is a general framework, which can improve the P–E tradeoff in the BSN regardless of the specific type of physiological signals. Without loss of generality, we choose four different types of biosignals [24] from Physionet [25] as our test bench in the experiments, electrocardiography (ECG), EEG, electromyography (EMG), and electrooculography (EOG). They are all the vital electrophysiological signals gathered to monitor human health status. The characteristics of each category of the biosignals are listed in Table II, and their waveforms are shown in Fig. 4. We can see that these four types of biosignals have significantly different patterns.

Considering that biosignals are usually sparse under the discrete wavelet transform (DWT) basis, we use inverse discrete wavelet transform (IDWT) as the sparsity-inducing transformation basis Ψ. All of our experiments use Bernoulli random variables as the sensing array and use the uniform quantization strategy.

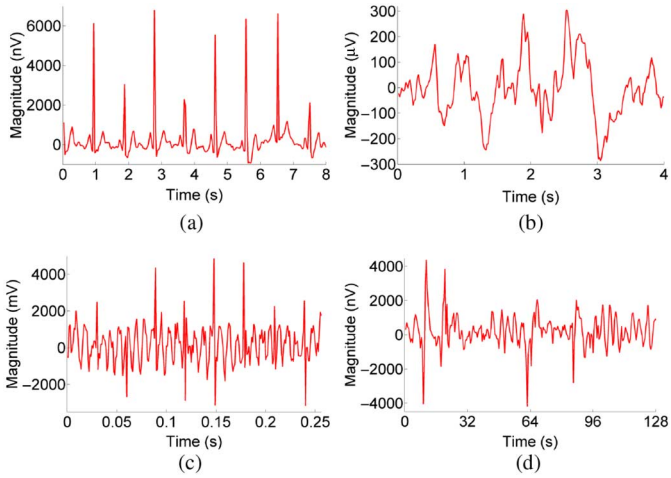

Fig. 4. Waveforms of the four biosignals from Physionet, and their patterns are significantly different. (a) ECG. (b) EEG. (c) EMG. (d) EOG.

TABLE II
Characteristics of Biosignals in the Testbench

Signal category	ECG	EEG	EMG	EOG
Sampling rate (Hz)	32	64	1000	2
Duration (s)	8	4	0.256	128
Magnitude unit	nV	μV	mV	nV
Magnitude range	[–936, 6792]	[–287, 304]	[–3160, 4864]	[–4184, 4378]

B. Energy Setup in Wireless Communication

We employ an ultralow-power transceiver model for wireless medical implant communications, which is proposed by Bohorquez *et al.* [26]. It includes a 350-μW MSK/FSK direct modulation transmitter and a 400-μW ON–OFF keying (OOK) super-regenerative receiver (SRR). The transceiver is implemented in 90-nm CMOS and digitally tunes 24 MHz in frequency steps smaller than 2 kHz. The transmitter meets the Medical Implant Communication Service (MICS) mask specifications [19] with data rates up to 120 kb/s consuming only 2.9 nJ/bit; the receiver has a sensitivity better than 93 dBm with a data rate of 120 kb/s consuming 3.3 nJ/bit. We are only concerned with the energy consumption on the sensor node. Therefore, to facilitate the calculation, we set the average energy consumption per bit of wireless communication (transmitter) as $C = 3$ nJ/bit.

C. Configurable QCS Versus Traditional CS

1) Energy-Efficiency Comparison: The significance of the configurable QCS architecture is that it takes into account the flexibility of resolution bit b in the quantization module. The experiment in this part is designed to explore how much the P–E tradeoff can be gained in our configurable QCS compared with the traditional CS architecture. In our experiment, we take all four biosignals for the benchmark evaluation. As shown in Fig. 4, there are no coherence features between any two signals in the time domain. Considering that the bit resolution requirement is usually high in the BSN application, we can set $b = 16$ for the traditional CS architecture during the experiment. For the QCS architecture, bit resolution ranges from 1 to 16. In the

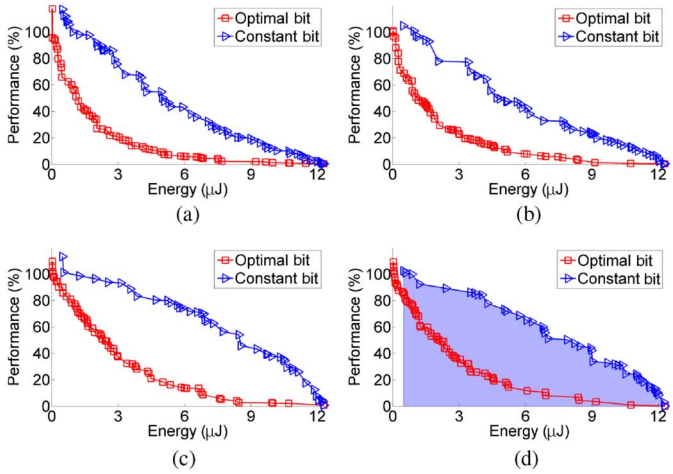

Fig. 5. (a)–(d) Pareto's curves of each signal. The blue area in (d) is an example of AUC. (a) ECG. (b) EEG. (c) EMG. (d) EOG.

experiment, we use the brute force method to find the Pareto's curve of the P–E space, and the results of four biosignals are shown in Fig. 5(a)–(d), respectively.

In Fig. 5(a)–(d), the red line is the Pareto's curve of the configurable QCS architecture, and the blue line is the Pareto's curve of the traditional CS architecture. Every marker, including red square and blue triangular, is an optimal P–E point. Here, we can see that the P–E tradeoff in the configurable QCS architecture is significantly better than that of the traditional CS architecture. For the constant bit case, ECG and EEG share a common approximately convex curve trend, while EMG and EOG appear as a concave shape. We can see that EMG and EOG signals gain more P–E tradeoff. More specifically, to quantitatively analyze the P–E gain, we adopt area under curve (AUC) [27] as our metric, which is the area between the Pareto's curve and the energy axis. The Pareto's curve consists of all optimal P–E tradeoff points, and these points form a set of trapezoidal areas. Therefore, we can add up all these areas and obtain AUC as follows:

$$\text{AUC} = \sum_i S_i \tag{23}$$

where i is the P–E point's number, S_i is the trapezoidal area between two adjacent P–E points of i and $i-1$, and the energy axis. For example, the AUC of the traditional CS architecture of the EOG signal is indicated as the blue area in Fig. 5(d). We can further define the tradeoff enhancement metric as follows:

$$\text{TO}_{\text{enhance}} = \frac{\text{AUC(CB)} - \text{AUC(OB)}}{\text{AUC(CB)}} \tag{24}$$

where AUC(CB) is the area of Pareto's curve of the traditional CS architecture, and AUC(OB) is the area of Pareto's curve of the configurable QCS architecture. According to (24), we can calculate the P–E tradeoff enhancement as in Table III.

From Table III, the improvements of P–E tradeoff are all more than 66% by considering bit resolution. It is indicated that our configurable QCS architecture can enhance the energy efficiency more than the traditional CS architecture. According to our enhancement definition, ECG gains the most efficiency

TABLE III
P–E TRADEOFF ENHANCEMENT TABLE

Signal category	ECG	EEG	EMG	EOG
AUC (CB)	1744.5	1781.3	2554.7	2344.5
AUC (OB)	437.5	537.5	843.8	788.0
$\text{TO}_{\text{enhance}}$ (%)	74.92	69.83	66.97	66.93

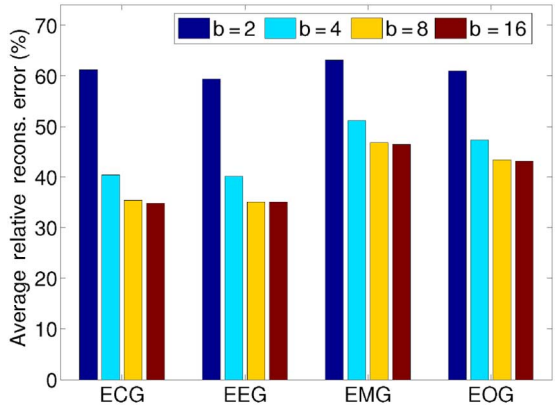

Fig. 6. Average relative reconstruction error over all possible energy bounds under different b setups.

and EOG gets the least improvement, which is contradictory with our previous observation. This is because our enhancement definition is an AUC ratio corresponding to the Pareto's curve of the traditional CS architecture. The AUC of EOG under the traditional CS architecture is much greater than that of other samples. Thus, its enhancement is down to the smallest sample. Overall, it seems that all four enhancements do not have significant difference, all about 70%, which indicates that our bit resolution strategy has similar impacts on different types of biosignals in BSN applications.

We also examine the reconstruction error under different bit resolution b setups to verify the good performance of the setup, $b = 16$, for the traditional CS architecture. We choose four setups of bit resolution, where $b = 2,\ 4,\ 8,$ and 16. For a specific energy bound and given b, we first calculate the relative reconstruction error using the reconstruction result of the constant bit subtracting that of the optimal bit case under the same energy bound. Then we calculate the average relative reconstruction error over all possible energy bounds for specific b setup. The related results are shown in Fig. 6. We can find that the average relative reconstruction error decreases rapidly from $b = 2$ to $b = 8$. The case of $b = 16$ always holds the minimal average relative reconstruction error for all the biosignals, which demonstrates the superiority of the setup $b = 16$ for the traditional CS with constant bit strategy.

2) Reconstructed Signal Comparison: In practical applications, precise reconstruction signals usually need post-processing. Thus, we would like to take a closer look at the signal quality, comparing between traditional CS and configurable QCS architecture in this experiment. We can directly check the related energy configuration and performance when setting an energy bound as $E_0 = 3.6$ μJ. All four reconstruction

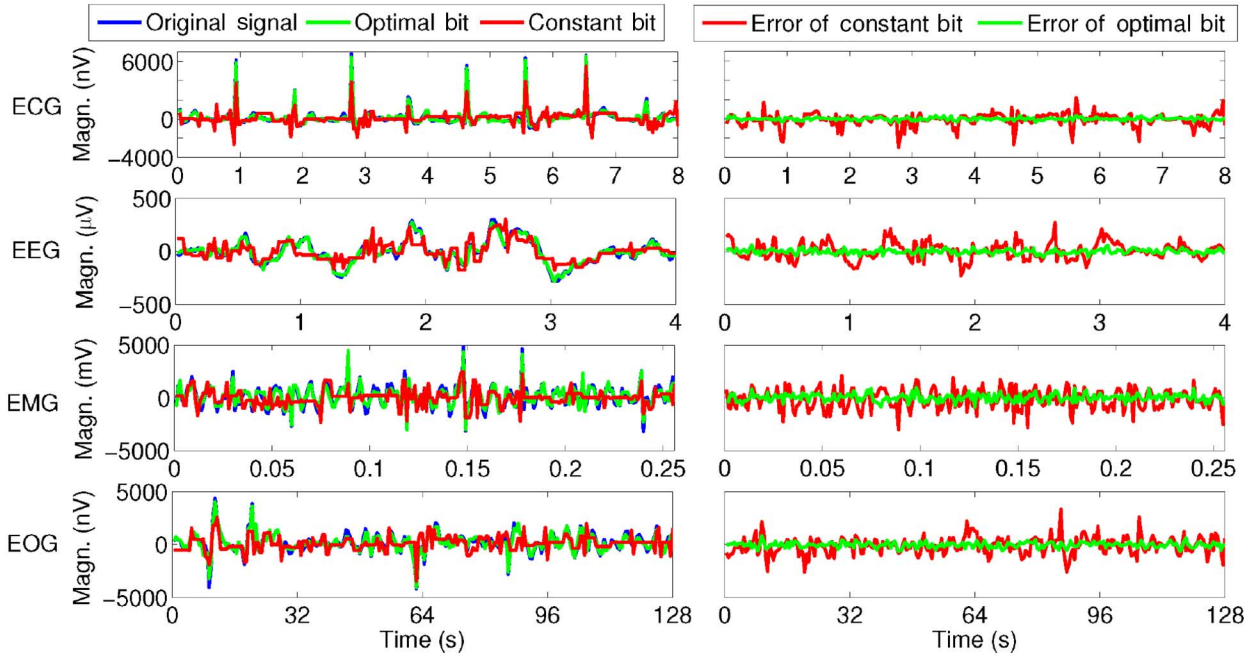

Fig. 7. Reconstructed waveforms of four biosignals when the energy bound is set as 3.6 μJ.

TABLE IV
ENERGY CONFIGURATION AND PERFORMANCE OF THE RECONSTRUCTED SIGNALS ON $E_0 = 3.6$ μJ

Signal Category		ECG	EEG	EMG	EOG
Configurable QCS	M	200	234	226	235
	b	6	5	5	5
	E (μJ)	3.600	3.510	3.390	3.525
	P (%)	**14.06**	**19.27**	**32.41**	**26.13**
Traditional CS	M	69	73	74	73
	b	16	16	16	16
	E (μJ)	3.312	3.504	3.552	3.504
	P (%)	**68.14**	**70.40**	**88.81**	**86.30**

waveforms are depicted in Fig. 7, and the detailed energy configurations with corresponding performance information on the energy bound are illustrated in Table IV.

There are two columns in Fig. 7. The left column indicates the reconstruction results of four biosignals, while the right column is the corresponding sample-level reconstruction error between the two CS architectures and the original signal. From the contrasting of the left column, we can see that our configurable QCS (green line) almost ideally covers the original signal (blue line). The reconstruction waveform of the traditional CS (red line) is with larger distortion than the configurable one. It is also obviously shown in the right column that the sample-level reconstruction error of our QCS is much smaller than the traditional CS. In all four biosignals, the traditional CS cannot reconstruct the peak part appropriately, which is always much smaller than the original signal, especially in ECG and EMG. For the relatively flat position in each signal, the reconstruction of traditional CS suffers from almost no changes, which is more significant in ECG and EMG, or larger fluctuations, as in EEG and EOG.

From Table IV, we can see that the performance of the traditional CS is all much larger than the configurable QCS. When we look at the energy configuration (M, b), we can find that the bit resolution in configurable QCS is 5 or 6, far away from 16 in the traditional CS. Although the total energy consumption in the two architectures is close, there is remarkable difference in the reconstruction error rate. Specifically, the performance difference between configurable QCS and traditional CS architecture in all four signals, ECG, EEG, EMG, and EOG, are about 50%–60%, resulting in an easy identification of their waveforms' differences. Also, ECG under the configurable QCS holds the least reconstruction error rate, 14.06%. We cannot find any significant distortion under this case. However, for EMG, its reconstruction error rate under traditional CS is up to 88.81%. The reconstructed result loses some salient information from the original EMG signal. The corresponding error rate under the configurable QCS is 32.41%, also the highest error rate in all of the QCS's reconstructions. This largest error rate results from the weak sparsity of EMG signals, seemingly with larger randomness, which indicates that DWT can not reconstruct with as high a quality as the other three signals.

D. Rapid Optimal Configuration With Energy Bound Budget in QCS

1) Performance Accuracy Analysis: In this experiment, we will demonstrate the performance of our RapQCS algorithm compared with the brute force method. We use all four types of biosignals. Their patterns are already shown in Fig. 4. Due to the requirement of the tuning phase in our RapQCS algorithm, we consider all three biosignals' combinations as the tuning applications, and the remaining signal under the corresponding case is the testing waveform. In this way, each signal is taken as testing data only once. For a comprehensive examination, we set energy bound on every discrete energy level. After the searching of our RapQCS algorithm, we can obtain

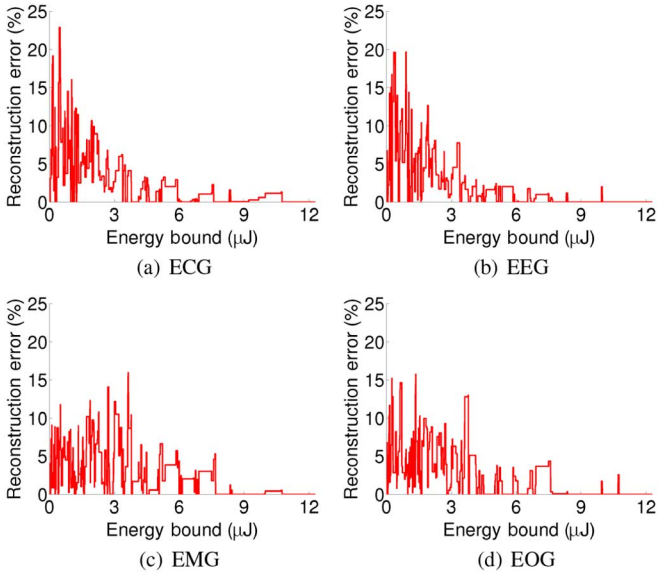

Fig. 8. Absolute reconstruction error between RapQCS curve and brute force curve. (a) ECG. (b) EEG. (c) EMG. (d) EOG.

an optimal RapQCS performance curve (i.e., RapQCS curve), with an optimal P–E tradeoff point on every energy bound. The absolute reconstruction difference between RapQCS curve and the brute force curve is illustrated in Fig. 8.

In Fig. 8, there are four subgraphs indicating the absolute reconstruction error between RapQCS curve and brute force curve, corresponding to four different categories of biosignals. The common trend among them is that the absolute error between these two types of curves decreases rapidly as energy bound increases. For all samples except EMG signal, the relatively larger errors always occur on the interval whose energy bound is less than 1.5 μJ. When energy bound increases more than 3 μJ, their absolute error will fluctuate in a relatively small range, less than 3%. On the low-energy bound, measurements number M and bit resolution b are both small. For ℓ_1 convex optimization problem, less M will result in large reconstruction error rate. It is reported that M should meet the following condition for a successful reconstruction:

$$M \geq K \log\left(\frac{N}{K}\right) \tag{25}$$

where K is the sparsity of input signal. Thus, even a small M may cause reconstruction failure. Smaller b introduces more quantization error into the reconstruction, which is always modeled by noise. Therefore, performance in a small energy interval takes on strong randomness, making our RapQCS method easily trapped in local minima. As energy increases, M and b both grow gradually. Less quantization error and more accurate convex optimization make the reconstruction error rate decrease rapidly and become more stable. Less local minima provide a larger chance for our algorithm to approximate to the optimal solution. For the EMG signal, its absolute error is relatively larger than other signals. In Fig. 4, the waveform of EMG is more like a random sequence. DWT is not good at dealing with such a signal. So the performance may engender more local minima to confuse our RapQCS method to reach its right destination.

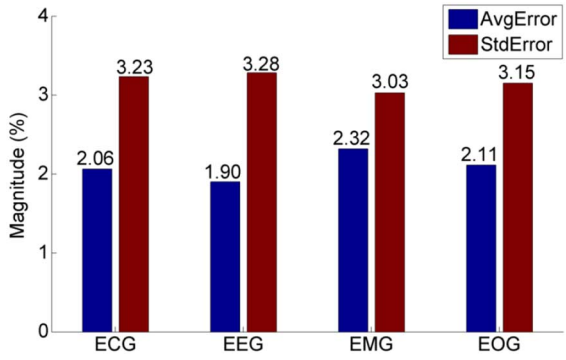

Fig. 9. Absolute reconstruction error of all four biosignals. AvgError presents the average absolute reconstruction error over all energy bounds. StdError presents the standard deviation of absolute reconstruction error over all energy bounds.

Specifically, we can use the average error rate AvgError and standard deviation StdError to quantitatively evaluate the reconstruction accuracy of our RapQCS algorithm. Because our performance has already been defined as a reconstruction error rate, we can calculate the average absolute error rate and standard deviation on all the energy bounds to indicate the overall error level

$$\text{AvgError} = \frac{1}{|\text{EB}|} \sum_{\text{eb}\in\text{EB}} \text{abs}(P_{\text{Rap}}(\text{eb}) - P_{\text{opt}}(\text{eb})) \tag{26}$$

$$\text{StdError} = \left(\frac{1}{|\text{EB}|} \sum_{\text{eb}\in\text{EB}} (\text{abs}(P_{\text{Rap}}(\text{eb}) - P_{\text{opt}}(\text{eb})) - \text{AvgError})^2\right)^{\frac{1}{2}} \tag{27}$$

where EB is the set of all energy bounds. $P_{\text{Rap}}(\text{eb})$ indicates the reconstruction error of RapQCS method under energy bound eb. $P_{\text{opt}}(\text{eb})$ is the optimal performance querying the brute force curve. The AvgError and StdError of all four signals are shown in Fig. 9.

From Fig. 9, our RapQCS method holds about a 2.0% average error rate in the general case except the EMG case. The standard deviations are all below 3.3%, which is a trivial fluctuation. As observed in Fig. 8, ECG, EEG, and EOG only suffer from larger error rates in a small low-energy bound interval, while they hold lower error rates on high-energy bound intervals. For the EMG signal, it has a larger average error rate of 2.32%, due to its problematic reconstruction. Even under this situation, the average level of all performance error rates is 2.10%, with about 3.17% standard deviation. We can see that the impact of reconstruction distortion affected by such subtle error rate can be nearly neglected. Therefore, when given a bound energy budget, our RapQCS algorithm can reach an accurate P–E tradeoff.

2) Energy Accuracy Analysis: In this part, we continue to check the energy accuracy between our RapQCS algorithm and the brute force algorithm. The absolute energy configuration error of these two algorithms is illustrated in Fig. 10.

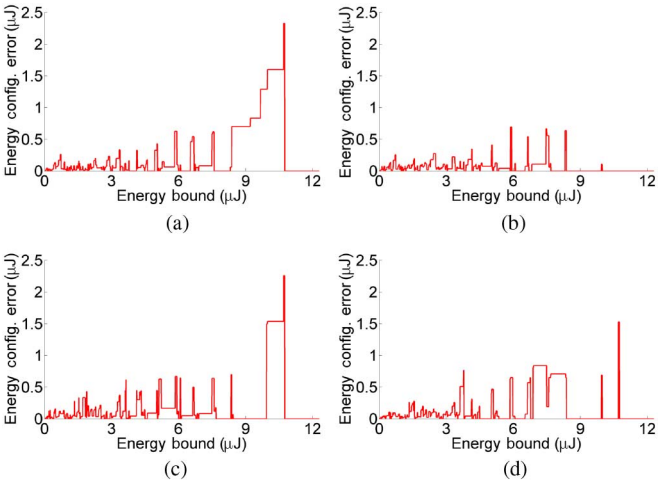

Fig. 10. Absolute energy configuration error between RapQCS algorithm and brute force algorithm. (a) ECG. (b) EEG. (c) EMG. (d) EOG.

Combining the trends of four biosignals, the absolute error is very small on the low-energy bound levels in Fig. 10. As energy bound increases, this error shows a growing trend. We can see that on high-energy bound, the absolute error is either very small or relatively large. The reason is that our P–E space consists of many discrete energy levels. As part of the energy definition in (10), the step length between two adjacent energy levels will increase as the energy increases. Thus, any inaccurate searching will result in a large absolute energy error.

In all of these four biosignals, EEG keeps an accurate configuration on high-energy bound levels, but the other three biosignals suffer from different degrees of deviation. On all energy bounds, the EMG signal shows relatively large fluctuation. Because our reconstruction algorithm cannot recover EMG signal well, its performance may take on strong randomness, which will result in more confusing local minima. Thus, the energy configuration of our RapQCS is with larger fluctuations. The ECG and EOG signals both have large energy configuration error on the higher energy bound levels. Also, when we take a closer look at the performance on high-energy bound in Fig. 8, their performances are all in a small range. This persuasively demonstrates the superiority of our configurable QCS architecture to exploit the energy efficiency. Specifically, we will still use the AvgError and StdError to evaluate the energy configuration accuracy of our RapQCS method. Since we already get the absolute energy error on every energy bound, these two indicators of all four signals can be directly calculated, as listed in Fig. 11.

Fig. 11 confirms our previous observation. The average absolute errors of ECG and EMG are relatively larger than other segments, more than 0.05 μJ. Their standard deviations are also much greater than others. The error of ECG is caused by the initial energy configuration setup. The EEG signal is with less average error and standard deviation than other signals, because the EEG has less energy configuration deviation on the larger energy level. Although there are some impacts caused by those factors, the average error rate of our results is only about 0.16 μJ, which is strongly supports the excellent energy accuracy of our RapQCS algorithm.

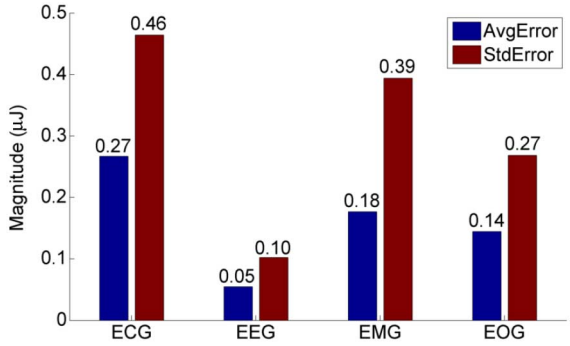

Fig. 11. Absolute energy configuration error of all four biosignals. AvgError presents the average absolute energy configuration error over all energy bounds. StdError presents the standard deviation of absolute energy configuration error over all energy bounds.

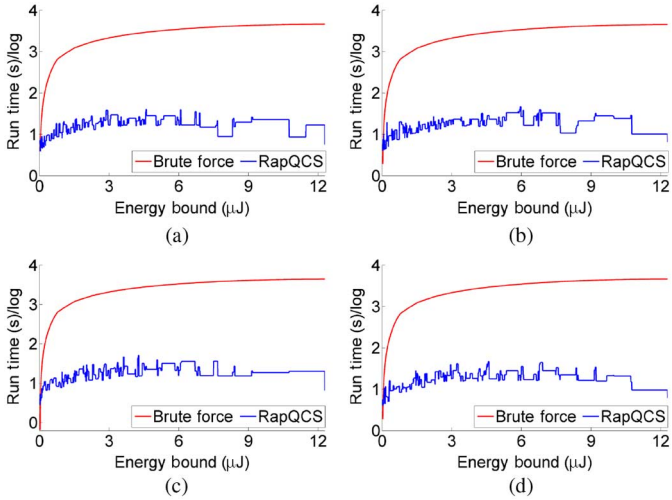

Fig. 12. Run-time comparison between RapQCS algorithm and brute force algorithm. (a) ECG. (b) EEG. (c) EMG. (d) EOG.

TABLE V
RUN TIME SPEEDUP BETWEEN BRUTE FORCE AND RAPQCS ALGORITHM

Signal category	ECG	EEG	EMG	EOG
A_{run} (BruteForce) (10^7)	1.29	1.26	1.24	1.29
A_{run} (RapQCS) (10^4)	7.49	7.98	8.15	7.78
Speedup	171.6×	157.9×	151.5×	166.1×

3) Run Time Analysis: Although the brute force method can find the optimal solution in P–E space, its huge computational burden is a main obstacle for practical applications. In this experiment, we will continue to explore the run time contrasts between the RapQCS method and brute force method. Also, we set energy bound on every energy level to do a comprehensive comparison. Related run time graphs are illustrated in Fig. 12. Because the run time difference between these two methods is large, about three orders of magnitude difference, we use the log axis of run time to show clearer details.

From Fig. 12, the run time of the brute force algorithm is increasing all the time. Its searching space first extends with a dramatically fast speed when energy bound is less than 1 μJ. Then run time increases by a small speed after energy bound

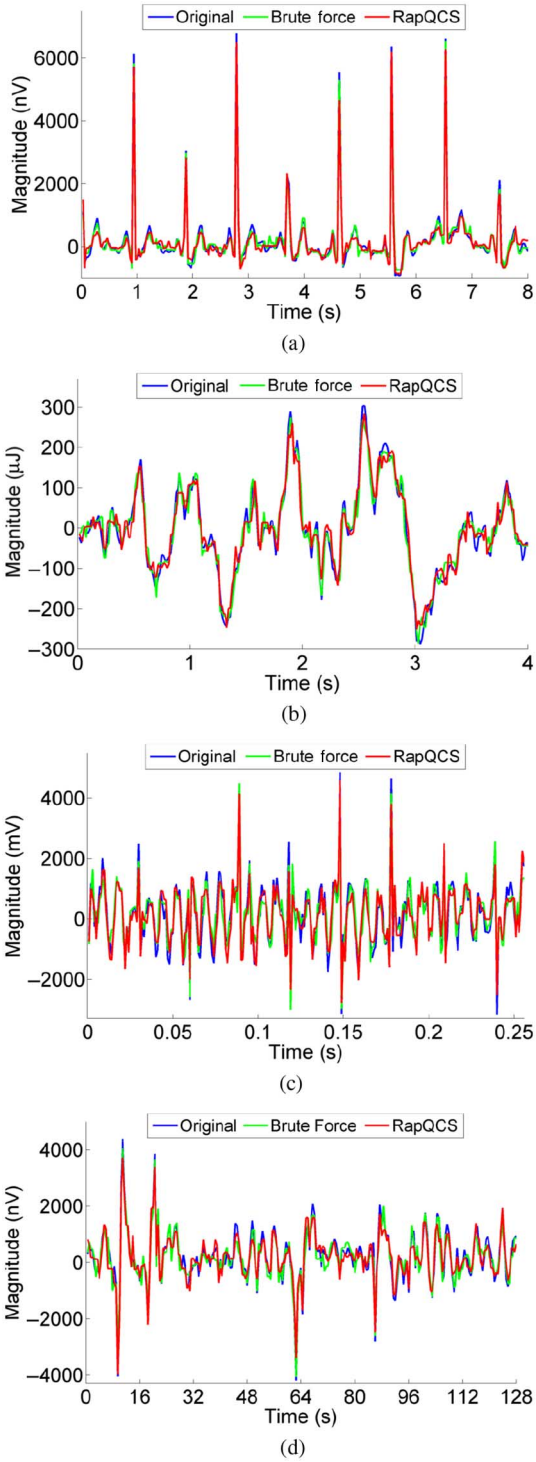

Fig. 13. Reconstruction results of all four biosignals on $E_0 = 3.6$ μJ. (a) ECG. (b) EEG. (c) EMG. (d) EOG.

1 μJ. Because we have no information on the energy bound value ahead of time, when we get the energy bound, the brute force method must search all the subspace, where energy is less than the given energy bound. However, our RapQCS method starts from its optimal initial configuration. So its solution can usually be found in several searching steps. This is a critical time-reducing factor. Like A_{PE} and $\text{TO}_{\text{enhance}}$ in Experiment *C-1*, we will introduce A_{run} and $\text{Speedup}_{\text{run}}$ to calculate the speedup quantitatively. A_{run} refers to the area between the run time curve and energy bound axis

$$A_{\text{run}} = \sum_i S_{\text{run}}(i) \tag{28}$$

where $S_{\text{run}}(i)$ is the trapezoidal area between two adjacent points in the run time curve and energy bound axis in the run-time–energy-bound axis, not the log run time axis as shown in Fig. 12. Therefore, we can define the time speedup as follows:

$$\text{Speedup}_{\text{run}} = \frac{A_{\text{run}}(\text{Brute Force})}{A_{\text{run}}(\text{RapQCS})}. \tag{29}$$

Table V shows the speedup of four biosignals. The speedup in all cases is more than 150 times without significant differences. This is because the run time of four biosignals using the brute force algorithm is similar. Our RapQCS method's run time fluctuates with a rising trend due to the initial energy configuration. Thus, the speedups have small waves. It is firmly demonstrated that our RapQCS algorithm provides significant improvement to the run time.

4) Case Study: In experiment *D-1*, we see the relationship between the performance of RapQCS's curve and Pareto's curve. In this experiment, we will take a closer look at the reconstruction results of our RapQCS algorithm, comparing them with an optimal solution and ground truth. The optimal solution indicates the optimal result from applying brute force to the P–E space, while ground truth is the original input signal. For a better comparison, we set an energy bound $E_0 = 3.6$ μJ. Their reconstruction results are shown in Fig. 13.

In Fig. 13, the blue line is the original input biosignal, the red line is our RapQCS's result and the green line is the reconstruction querying from the brute force curve. For all four biosignals, the patterns from the RapQCS algorithm and brute force curve are very similar to each other. We cannot directly identify which performance is better between the two methods. They all approximate to the ground truth closely. Therefore, we investigate their detailed information, the energy configuration, and performance, as listed in Table VI.

We observe that the absolute performance error rates of the four signals are all below 6%. This demonstrates the similar reconstruction signals between our RapQCS case and optimal case. For EMG, although the performance difference of the two reconstructions is only 3.6%, their own performances are both larger than the other three signals, according to Table VI.

TABLE VI
COMPARISON OF CONFIGURATION, ENERGY, AND PERFORMANCE BETWEEN RAPQCS AND OPTIMAL RECONSTRUCTION

Signal category		ECG	EEG	EMG	EOG
RapQCS reconstruction	M	232	231	234	228
	b	5	5	5	5
	E (μJ)	3.480	3.465	3.510	3.420
	P (%)	17.47	21.82	36.01	32.17
Optimal reconstruction	M	200	234	226	235
	b	6	5	5	5
	E (μJ)	3.600	3.510	3.390	3.525
	P (%)	14.06	19.27	32.41	26.13

The energy bound setup is $E_0 = 3.6$ μJ.

Overall, it is strongly supported that our RapQCS algorithm can quickly approximate the optimal P–E tradeoff.

VII. Conclusion and Future Work

In this paper, we present a configurable QCS architecture, which jointly considers the configuration of sampling rate and quantization in its framework to further more optimize the CS process in real-life applications. Through a case study on the application of BSNs, our experimental results indicate that the configurable QCS architecture can provide more than 66% P–E tradeoff gain than the traditional CS architecture. Also, we proposed a rapid configuration algorithm, RapQCS, for the configurable QCS architecture. In experiments, our proposed RapQCS algorithm can reach more than $150\times$ speedup, while only decreasing the signal fidelity by 2.32%.

In the future, we will further explore the design space within the configurable QCS architecture. For example, in addition to the bit resolution, we will also investigate the nonuniform quantization strategies. Also, we will investigate better construction algorithms and transformation basis for complex signals, such as the EMG signal in this experiment.

References

[1] S. Li, L. Da Xu, and X. Wang, "A continuous biomedical signal acquisition system based on compressed sensing in body sensor networks," *IEEE Trans. Ind. Informat.*, vol. 9, no. 3, pp. 1764–1771, Aug. 2013.

[2] S. J. Lee, Y. Motai, and H. Choi, "Tracking human motion with multichannel interacting multiple model," *IEEE Trans. Ind. Informat.*, vol. 9, no. 3, pp. 1751–1763, Aug. 2013.

[3] H.-C. Lin, S.-Y. Chiang, K. Lee, and Y.-C. Kan, "An activity recognition model using inertial sensor nodes in a wireless sensor network for frozen shoulder rehabilitation exercises," *Sensors*, vol. 15, no. 1, pp. 2181–2204, 2015.

[4] X. Wang, Q. Gui, B. Liu, Z. Jin, and Y. Chen, "Enabling smart personalized healthcare: A hybrid mobile-cloud approach for ECG telemonitoring," *IEEE J. Biomed. Health Informat.*, vol. 18, no. 3, pp. 739–745, May 2014.

[5] A. Wang, Z. Jin, C. Song, and W. Xu, "Adaptive compressed sensing architecture in wireless brain-computer interface," in *Proc. 52nd Annu. Des. Automat. Conf.*. 2015, p. 173.

[6] D. L. Donoho, "Compressed sensing," *IEEE Trans. Inf. Theory*, vol. 52, no. 4, pp. 1289–1306, Apr. 2006.

[7] E. J. Candes and T. Tao, "Near-optimal signal recovery from random projections: Universal encoding strategies?" *IEEE Trans. Inf. Theory*, vol. 52, no. 12, pp. 5406–5425, Dec. 2006.

[8] M. F. Duarte *et al.*, "Single-pixel imaging via compressive sampling," *IEEE Signal Process. Mag.*, vol. 25, no. 2, p. 83, Mar. 2008.

[9] J. Wright, A. Y. Yang, A. Ganesh, S. S. Sastry, and Y. Ma, "Robust face recognition via sparse representation," *IEEE Trans. Pattern Anal. Mach. Intell.*, vol. 31, no. 2, pp. 210–227, Feb. 2009.

[10] S. Qaisar, R. M. Bilal, W. Iqbal, M. Naureen, and S. Lee, "Compressive sensing: From theory to applications, a survey," *J. Commun. Netw.*, vol. 15, no. 5, pp. 443–456, 2013.

[11] B. Liu, Z. Zhang, G. Xu, H. Fan, and Q. Fu, "Energy efficient telemonitoring of physiological signals via compressed sensing: A fast algorithm and power consumption evaluation," *Biomed. Signal Process. Control*, vol. 11, pp. 80–88, 2014.

[12] W. Dai, H. V. Pham, and O. Milenkovic, "A comparative study of quantized compressive sensing schemes," in *Proc. IEEE Int. Conf. Symp. Inf. Theory*, 2009, vol. 1, pp. 11–15.

[13] J. N. Laska, P. T. Boufounos, M. A. Davenport, and R. G. Baraniuk, "Democracy in action: Quantization, saturation, and compressive sensing," *Appl. Comput. Harmon. Anal.*, vol. 31, no. 3, pp. 429–443, 2011.

[14] J. Z. Sun and V. K. Goyal, "Optimal quantization of random measurements in compressed sensing," in *Proc. IEEE Int. Symp. Inf. Theory*, 2009, pp. 6–10.

[15] S. Fauvel and R. K. Ward, "An energy efficient compressed sensing framework for the compression of electroencephalogram signals," *Sensors*, vol. 14, no. 1, pp. 1474–1496, 2014.

[16] G. Li, Z. Ma, and F. Wang, "An approximate ℓ_0 norm based signal reconstruction algorithm in the compressive sampling theory," in *Proc. IEEE 6th Int. Conf. Awareness Sci. Technol. (iCAST)*, 2014, pp. 1–5.

[17] A. M. Tillmann and M. E. Pfetsch, "The computational complexity of the restricted isometry property, the nullspace property, and related concepts in compressed sensing," *IEEE Trans. Inf. Theory*, vol. 60, no. 2, pp. 1248–1259, Feb. 2014.

[18] A. Wang, W. Xu, Z. Jin, and F. Gong, "Quantization effects in an analog-to-information front end in EEG telemonitoring," *IEEE Trans. Circuits Syst. II. Exp. Briefs*, vol. 62, no. 2, pp. 104–108, Feb. 2015.

[19] P. Soontornpipit, "Design of an implantable antenna feasibility study for continuous glucose monitoring," *ECTI Trans. Elect. Eng. Electron. Commun.*, vol. 12, no. 1, pp. 44–52, 2014.

[20] *IEEE Standard for Local and Metropolitan Area Networks—Part 15.6: Wireless Body Area Networks*, IEEE Standard 802.15.6, 2012.

[21] I. Kacem, S. Hammadi, and P. Borne, "Pareto-optimality approach for flexible job-shop scheduling problems: Hybridization of evolutionary algorithms and fuzzy logic," *Math. Comput. Simul.*, vol. 60, no. 3, pp. 245–276, 2002.

[22] M. S. Lobo, L. Vandenberghe, S. Boyd, and H. Lebret, "Applications of second-order cone programming," *Linear Algebra Appl.*, vol. 284, no. 1, pp. 193–228, 1998.

[23] Y.-X. Yuan, "Step-sizes for the gradient method," *AMS IP Stud. Adv. Math.*, vol. 42, no. 2, p. 785, 2008.

[24] R. Matthews, N. J. McDonald, P. Hervieux, P. J. Turner, and M. A. Steindorf, "A wearable physiological sensor suite for unobtrusive monitoring of physiological and cognitive state," in *Proc. 29th Annu. Int. Conf. IEEE Eng. Med. Biol. Soc.*, 2007, pp. 5276–5281.

[25] G. B. Moody, R. G. Mark, and A. L. Goldberger, "Physionet: A web-based resource for the study of physiologic signals," *IEEE Eng. Med. Biol. Mag.*, vol. 20, no. 3, pp. 70–75, May/Jun. 2001.

[26] J. L. Bohorquez, A. P. Chandrakasan, and J. L. Dawson, "A 350 μW CMOS MSK transmitter and 400 μW OOK super-regenerative receiver for medical implant communications," *IEEE J. Solid-State Circuits*, vol. 44, no. 4, pp. 1248–1259, Apr. 2009.

[27] S. Wang, D. Li, N. Petrick, B. Sahiner, M. G. Linguraru, and R. M. Summers, "Optimizing area under the ROC curve using semi-supervised learning," *Pattern Recognit.*, vol. 48, no. 1, pp. 276–287, 2015.

Aosen Wang (S'15) photograph and biography not available at the time of publication.

Feng Lin (M'15) photograph and biography not available at the time of publication.

Zhanpeng Jin (S'08–M'11) photograph and biography not available at the time of publication.

Wenyao Xu (M'14) photograph and biography not available at the time of publication.